A Coupled Multibody – Mid Fidelity Aerodynamic Tool for the Simulation of Tiltrotor Manoeuvres

Alberto Savino*, Alessandro Cocco, Andrea Zanoni, Alex Zanotti, Vincenzo Muscarello
Politecnico di Milano, Milano — Italy
* alberto.savino@polimi.it

Abstract
A nonlinear aeroelastic numerical tool was used in the present work for the evaluation of loads and vibratory levels of a tiltrotor aircraft during critical transient manoeuvres. The numerical tool applicable to fixed and rotary-wing aircraft was obtained by joining the multibody solver MBDyn and the mid-fidelity aerodynamic tool DUST, through the partitioned multi-physics coupling library preCICE. The aim of this work was to assess the ability of the nonlinear approach implemented in the coupled MBDyn-DUST tool for the simulation of tiltrotor aerodynamics and dynamics during a roll manoeuvre to be used for the preliminary design of novel tiltrotor configurations. This activity was performed in the framework of the EU funded CleanSky 2 FORMOSA project, aimed to the design of a novel wing movable surface system for the NextGen Civil Tiltrotor aircraft.

1 INTRODUCTION

Tiltrotor design represents a challenging task for engineers, considering the multipurpose missions that are expected to be accomplished by this rather complex aircraft. In particular, tiltrotors must be able to take-off and landing as helicopters and perform a conversion manoeuvre of rotors to flight as an airplane. In order to efficiently control these vehicles, wing movables surfaces and actuation systems are driven by a complex Flight Control System (FCS) capable to mix the action control during the different flight conditions that characterise this aircraft mission [1, 2]. Control surfaces and actuators selection require a correct evaluation of aeroelastic loads during manoeuvres in order to improve the vehicle response, increase the efficiency and reduce the weight and complexity of control system.

High–fidelity aerodynamic solvers were typically used to explore the complex interactions between rotors wake and wing that are peculiar of the different attitudes reproduced by these aircraft during their flight mission. Nevertheless, the computational cost of high-fidelity CFD simulations for such configurations precludes their applications to a limited number of vehicle configurations. Consequently, in recent years the interest about mid-fidelity aerodynamic solvers based on vortex particle method (VPM) [3] has grown in rotorcraft research field. From dynamics point of view, tiltrotor manoeuvres are typically investigated through a multibody approach, which takes into account the nonlinear dynamics of interconnected bodies representing tiltrotor components during the transients [4]. The multibody approach is also used to investigate aeroelastic phenomena, especially in airplane mode flight, where whirl flutter instabilities may occur [5]. In the present work, a medium fidelity aerodynamics and multibody approaches have been joined to obtain a useful tool which aims at an effective trade-off to obtain fast and accurate solutions that can be used for tiltrotor aeroelastic analysis.

DUST [6] and MBDyn [7] were coupled by using the Python library preCICE [8]. The coupling has been tested using simple aeroelastic models and subsequently was used to predict aeroelastic stability margins in tiltrotor aircraft, and to simulate transient manoeuvres such as rotor-nacelle conversion and roll manoeuvres in airplane mode flight. A thorough validation of the capabilities of DUST to capture interactional effects between rotor and wing in hover, cruise and conversion mode for tiltrotor configurations was performed in recent works [9, 10]. The present work shows the validation of the coupled tool on a fixed and a rotary wing applications. Then, coupled MBDyn-DUST simulations were performed to show the importance of an accurate simulation of rotors-wing aerodynamic interaction on aircraft performances during a roll manoeuvre. In particular, this effect is of particular importance for tiltrotors that are characterized by wings with low aspect ratios subjected to rotors wake influence along a large portion of wing span.

2 COUPLED MBDYN-DUST TOOL

The coupled multibody-aerodynamic tool exploits the two codes, MBDyn and DUST, for the resolution of the structural and aerodynamic problem respectively. The commu-

Presented at the 47th European Rotorcraft Forum, Glasgow, UK, 7-10 September, 2021

nication between the two software is performed through preCICE, which is an open-source software released under the LGPL3 license and available on GitHub (`https://github.com/precice/precice`) [8]. preCICE (Precise Code Interaction Coupling Environment), is a coupling library for partitioned multi-physics simulations capable of simulating a subpart of the complete physics involved in a simulation. An adapter for MBDyn software has been implemented to allow the communication of all kinematic variables (i.e. position, orientation, velocity and angular velocity) and forces and moments acting on the nodes of a MBDyn model exposed through an external structural force.

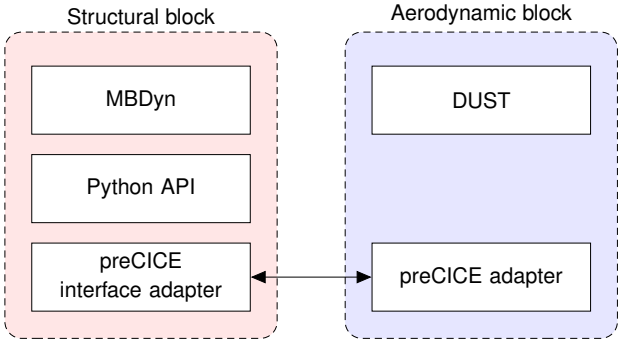

Figure 1: Communication managed through the two solvers adapters

Figure 1 shows the communication and information exchange, managed through the two solvers. A detailed description of the implementation of software coupling can be found in [11].

2.1 Validation of the aeroelastic tool

2.1.1 Goland Wing

Firstly, the coupling between MBDyn and DUST has been validated on the Goland wing test case [12]. In particular, the flutter speed prediction of the code was tested for a low-aspect ratio wing test case where the impact of three-dimensional aerodynamics is consistent. The structural model of the wing was built using four beams with a C^0 discretization based on the finite volume concept presented by [13]. The number of beams was obtained by imposing a convergence requirement on the first four modes reported by Goland [12], see Tab. 1.

	Goland et al. [12] Hz	MBDyn Hz
1^{st} Bending	7.66	7.66
1^{st} Torsion	15.24	15.21
2^{nd} Bending	38.80	38.54
2^{nd} Torsion	55.33	54.79

Table 1: Comparison on the first four natural frequencies computed for the Goland wing.

A quite good agreement with results obtained in literature by different aeroelastic solvers was found for the flutter speed computed by MBDyn-DUST simulations, as can be observed from Tab. 2. Moreover, Fig. 2 reported the time history of the vertical displacement of the wing tip computed by MBDyn-DUST simulations for three flight speeds around the flutter point, considering the panel mesh case. A visualization of the Goland's wing flexural–torsional flutter mode computed at 200 m/s flight speed is shown in Fig. 3.

Author	V_f, $\mathrm{m\,s^{-1}}$	ω_f, $\mathrm{rad\,s^{-1}}$
Wang et al. [14]	174.3	-
Wang et al. [14]	163.8	-
SHARP et al. [15]	165.0	69
MBDyn-DUST	168.2	68.11
MBDyn-DUST	174.2	69.49

Table 2: Comparison of flutter speed computed for the Goland wing.

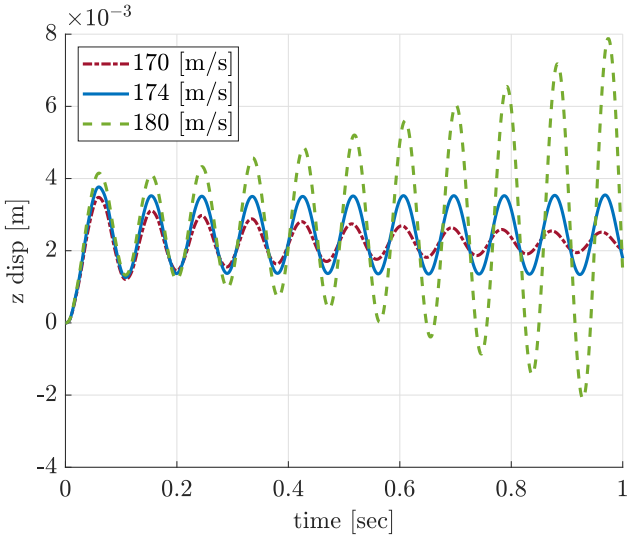

Figure 2: Time history of vertical displacement of the wing tip for panel aerodynamic mesh.

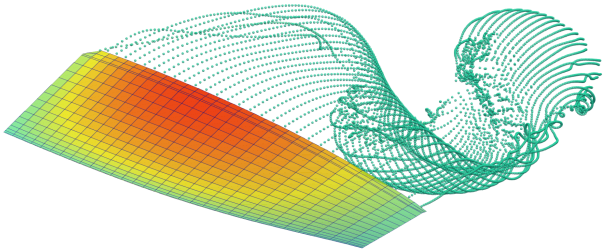

Figure 3: Visualization of Goland's wing flutter mode at 200 m/s flight speed.

2.1.2 XV–15 Rotor

The rotary wing test case used for MBDyn-DUST tool validation was the XV–15 rotor equipped with flexible metal blades. The XV–15 proprotor is a three bladed stiff-in-plane rotor with a gimballed hub. The multibody model of the control chain shown in Fig. 4 and Fig. 6 was built using information contained in [16]. The role of each component is the following:

- `Pylon`: this node represents the actual connection between the pylon extremity and the rotor; when the isolated rotor is analyzed this node is clamped.
- `Airframe`: this node is the one to which the commands (cyclics and collective) are imposed, in order to decouple the two cyclic inputs the node is positioned on a reference system that is rotated by the angle $\psi_{sp} = atan\left(\frac{x_{sp}}{y_{sp}}\right)$ where x_{sp} and y_{sp} are the location of the pitch link attachment to the swashplate.
- `Fixed Swashplate`: this node is rigidly constrained in the in–plane translations and the axial rotation to the airframe. To account for the flexibility of the control chain it is connected to the airframe by three equally radially spaced rods.
- `Rotating Swashplate`: this node is connected to the fixed swashplate by means of a revolute hinge; it is positioned on a rotating reference system.
- `Collective Head`: this node is connected to the airframe by means to a deformable spring in the vertical direction, in order to account for the flexibility for the collective path; it is positioned on a rotating reference system.
- `Head Rocket Arm`: this node is connected to the collective head through a revolute hinge, and to the rotating swashplate by means of a rod (cyclic tube). Then though the pitch link the cyclic and collective commands are transmitted to the blade.
- `Engine`: this node is connected to mast by means of a torsional spring in order to reproduce the drive-train dynamics.
- `Mast`: this node transmits the rotation to the hub and to the rotating swashplate. It is connected to the pylon node by means of a revolute hinge.
- `Hub`: This node is constrained to the mast node by means of a spherical hinge and a MBDyn gimbal rotation: the combination of these two joints allows the creation of an ideal constant velocity joint.
- `Yoke`: This component represent the flexbeam that connects the hub and the blade. The blade–to–yoke connection is performed by means of a dual load path connection in which the inner bearing is modelled as an inline joint, whereas the outer bearing is modelled as a spherical joint.

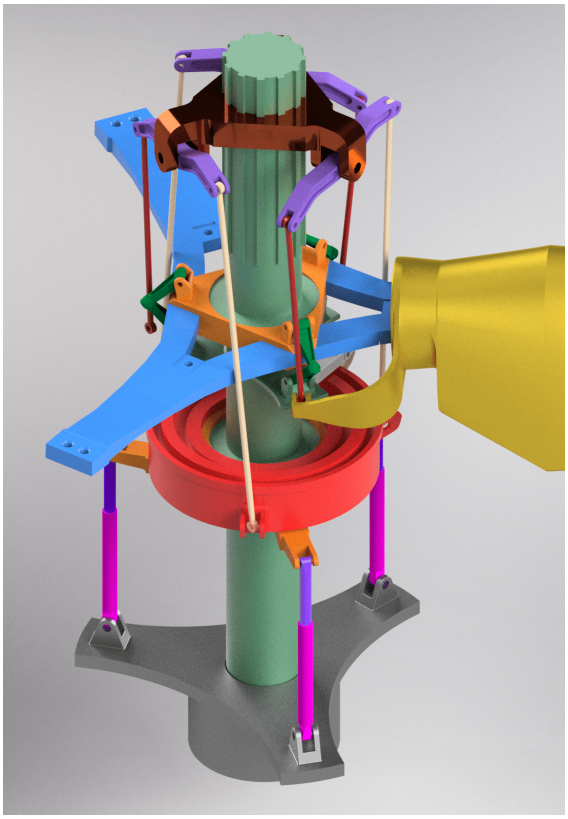

Figure 4: Layout of the XV-15 rotor control chain.

Each blade was modelled using 10 MBDyn three node finite volume beam elements [17] and each flexbeam by 4 three node beam elements. All rotor data are taken from the original CAMRAD II model presented in [18]. Table 3 reports the main rotor data, while Tab. 4 shows the blade airfoil distribution along the span, taken from [19].

Rotor data		
Blade	3	
Solidity	0.0891	
Radius	3.81	m
Precone β	2.5	deg
Chord	0.3556	m
Twist	45	deg
Nominal speed	589	RPM

Table 3: XV-15 Rotor main data.

Airfoil data		
Profile	start	end
Naca 64-935	0.09	0.13
Naca 64-528	0.13	0.34
Naca 64-118	0.34	0.655
Naca 64-(1.5)12	0.655	0.9
Naca 64-208	0.9	1

Table 4: XV-15 Blade airfoil distribution.

In the MBDyn alone model, aerodynamics is modelled through MBDyn aerobeams which implement a strip theory aerodynamic description with an appropriate tip loss model correction. On the other hand, for the coupled simulations, aerodynamics of each blade is modelled by DUST lifting line elements, naturally encompass both compressibility and viscous effects [9]. This aerodynamic model provides accurate result on high aspect ratio bodies as blades, while being computationally very efficient, as shown in [6]. While MBDyn model applies a non-smooth transition between adjacent airfoils sections, DUST interpolates the aerodynamic properties of the airfoils sections used to build the blade model. The dynamic behaviour of the rotor multibody model is shown by the fanplot computed at 0° collective shown in Fig. 5a, where MBDyn results are compared against CAMRAD II and RCAS results provided by [20]. The major differences between the three models are located on the third flap mode (3D) where the frequency of MBDyn are the softest between the three models. Nevertheless, a quite good agreement is obtained for almost all the frequencies.

Figure 5b shows the thrust coefficient C_T versus torque coefficient C_Q curves computed for the XV-15 rotor in hover with MBDyn alone and the coupled MBDyn-DUST simulation compared to experimental data reported in [19]. The quite higher agreement of the MBDyn-DUST simulation curve with experimental polar with respect to the MBDyn alone curve, particularly at high thrust coefficients, indicates the suitability of the coupled tool for an accurate simulation of rotor performance.

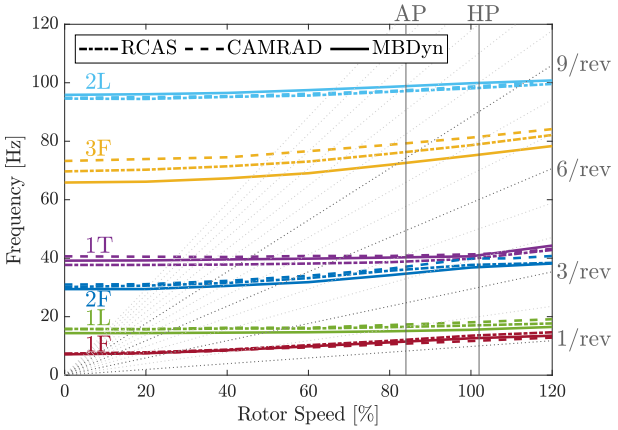

(a) XV-15 rotor fanplot in vacuum 0° – Collective Modes: comparison between MBDyn, CAMRAD II and RCAS models [20].

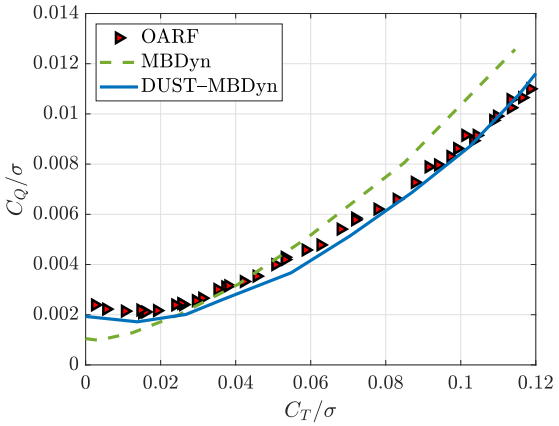

(b) XV-15 rotor torque coefficient over solidity C_Q/σ vs thrust coefficient over solidity C_T/σ: comparison between experimental and numerical data.

3 ROLL MANOEUVRE SIMULATIONS

In the present work a full-span aeroelastic model representative of the Bell XV-15 research aircraft equipped with metal blades [18] and thick wing case was considered for the roll manoeuvre simulations.

3.1 Aerodynamic model

The aerodynamic model exploits different formulations of aerodynamic elements such as lifting lines and surface panels. While lifting line aerodynamic elements are used for the rotor blades, the other components such as wing, tail, nacelles and fuselage are modelled by surface panels. The aerodynamic mesh of the full XV-15 tiltrotor is shown in Fig. 7.

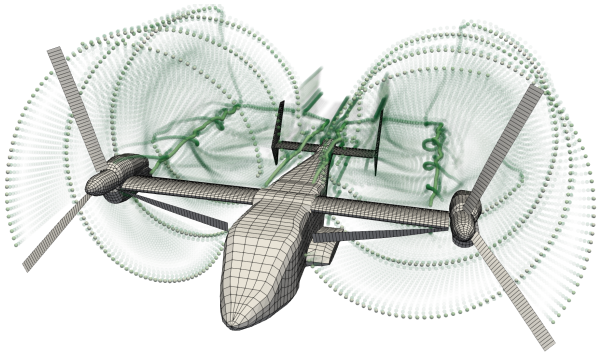

Figure 7: XV–15 full-scale aerodynamic mesh and free wake evolution

In order to simulate the aircraft manoeuvre, DUST models the wing control surfaces by deflecting a proper region of the aerodynamic mesh. Considering a two-dimensional representation, see Fig. 8, the control surface can be defined in the local reference frame of the component by

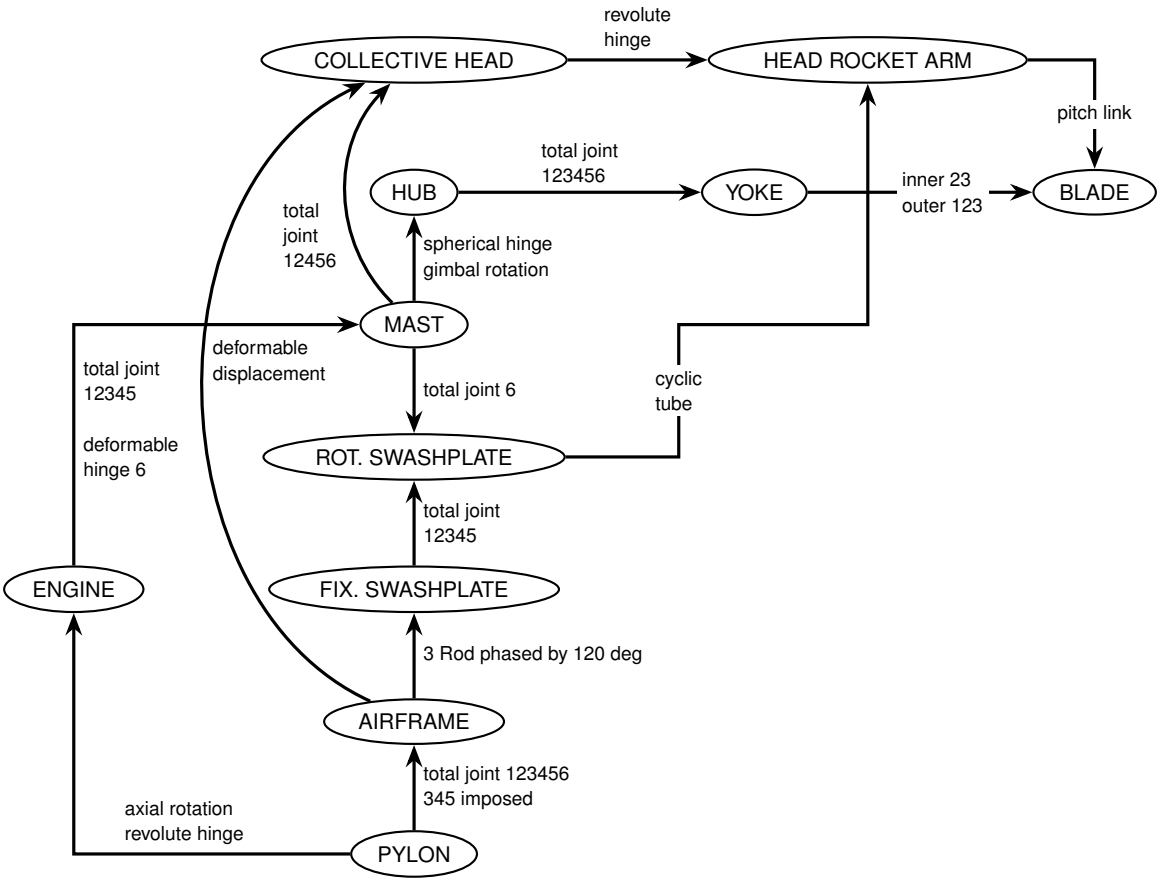

Figure 6: Flowchart indicating the individual blade pitch control system components and their connections for dual control path

means of the hinge axis position H, the chordwise direction ξ, the dimension of a blending region $[-u,u]$ introduced to avoid irregular behavior of the mesh along with the rotation angle θ. Thus, the rotation axis, $\hat{\boldsymbol{h}}$, is assumed orthogonal to the plane of the airfoil. A hinge orthonormal reference frame is defined with origin H, and axes ξ', $\hat{\boldsymbol{n}} = \hat{\boldsymbol{z}} \times \hat{\boldsymbol{v}}$. The position of a point w.r.t. this reference frame reads

$$\boldsymbol{r} = v\hat{\boldsymbol{\xi}} + n\hat{\boldsymbol{\eta}} + h\hat{\boldsymbol{h}} \,. \tag{1}$$

Three regions are defined using the coordinates defined through this reference frame:

1. $v \leq -u$: no influence of the aileron rotation

2. $v \geq u$: rigid rotation around the hinge

$$\Delta\boldsymbol{r} = \sin\theta\hat{\boldsymbol{h}} \times \boldsymbol{r} + (1-\cos\theta)\hat{\boldsymbol{h}} \times \hat{\boldsymbol{h}} \times \boldsymbol{r} \tag{2}$$

3. $-u \leq v \leq u$: blending region for avoiding irregular behavior defined as an arc of a circle connecting the fixed and deflected part.

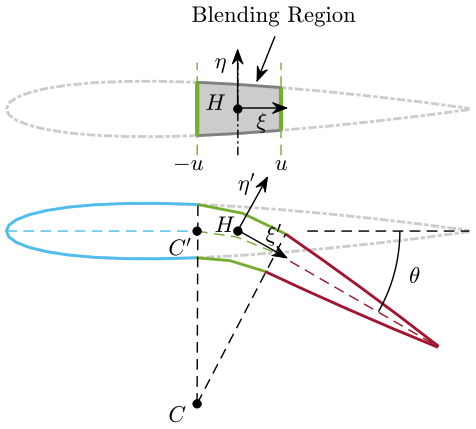

Figure 8: Sketch of control surface deflection modelling.

The rotation of each hinge node should be driven by a prescribed law of motion in the case of simple DUST model or it follows a structural node, in the case of coupled simulation.

3.2 Multibody model

The dynamic model setup includes:

- the wing, modeled as a rigid rigid body, including flaps and flaperons;
- the fuselage and the empennages, modeled as rigid bodies, including the rudders and the elevator control surfaces;
- the pylon/nacelle system, attached to the wing-tip; its tilting with respect to the wing can be driven to model the tiltrotor in airplane mode (APMODE), helicopter mode (HEMODE) or in any intermediate configuration;
- the rotor with the exact kinematics of the blade pitching mechanism.

The modelled rotor control chain was already presented in Sec. 2.1.2, while the blades are considered rigid in order to simplify the model. This simplification is considered legitimate since the purpose of this analysis is to study the roll maneuver characterized by low-frequency modes typical of flight mechanics. The model is grounded by locking all degrees of freedom with the exception of the rotation around the roll axis.

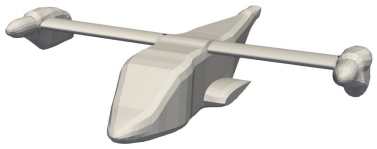

(a) Configuration I

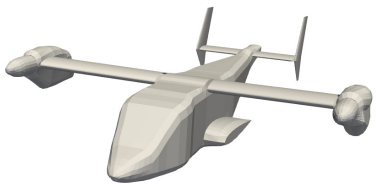

(b) Configuration II

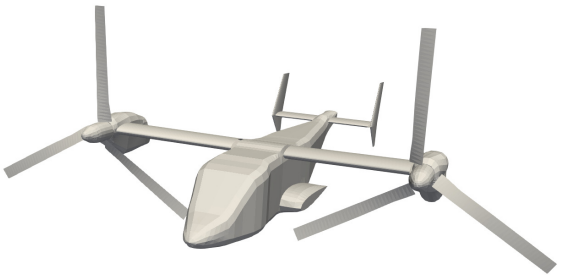

(c) Configuration III

Figure 9: Geometry of aircraft configurations tested for roll manoeuvre coupled simulations

3.3 Results and discussion

In order to evaluate the aerodynamic effect of tailplanes and rotor wake interaction on roll performance, coupled simulations were performed on three different aircraft configurations. As indicated in Tab. 5 and illustrated in Fig. 9, firstly the airframe only was considered, then the model complexity was increased by adding tailplanes and rotors. The structural model and the relative mass properties are the same for all the three configurations.

Configuration	Airframe	Tail	Rotor
Configuration I	✓	✗	✗
Configuration II	✓	✓	✗
Configuration III	✓	✓	✓

Table 5: Aircraft configurations tested for roll manoeuvre coupled simulations.

A trimmed flight condition reported by [21] was considered for the roll manoeuvre coupled simulations. The flight condition parameters are reported in Tab. 6. In the roll maneuver simulations the flaperons deflection δ_a follows a step function from 0° to $\pm 20^\circ$. The control surfaces start moving after 0.5sec from the beginning of the simulation to warrant that the manoeuvre starts when aerodynamic transients vanished. At the same time, the roll degree of freedom of the entire model is unlocked. The aircraft rolls around longitudinal axis directed positively with the starboard (right) wing up. Yawing rotation is around vertical body axis, directed positively with nose to left. Pitching rotation is around the axis perpendicular to the longitudinal plane of symmetry, directed positively nose up.

Flight Conditions		
Air density	1.225	$\mathrm{kg\,m^{-3}}$
Speed	72.022	$\mathrm{m\,s^{-1}}$
Trim parameters		
Mode	Airplane	
Pitch angle	6.944	deg
Rotor speed	517	RPM
Rotor collective	29.5015	deg
Elevator	-1.2398	deg

Table 6: Flight condition parameters used for roll manoeuvre simulation.

Figure 10 shows the comparison of the evolution of the bank angle ϕ during the simulated roll manoeuvre for the three aircraft configuration tested. In particular, time evolution of bank angle clearly shows that the introduction of aerodynamics effects due to tailplanes and rotor wakes change the slope of the curve and the roll manoeuvre performance. A representation of the effect of rotors wake with respect to aircraft configuration equipped with tailplanes is illustrated in Fig. 12.

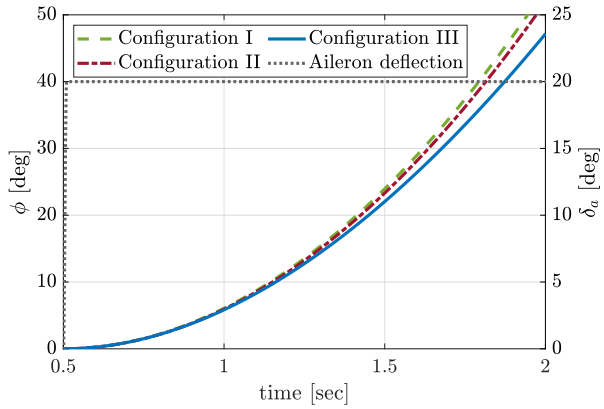

Figure 10: Comparison on bank angle evolution.

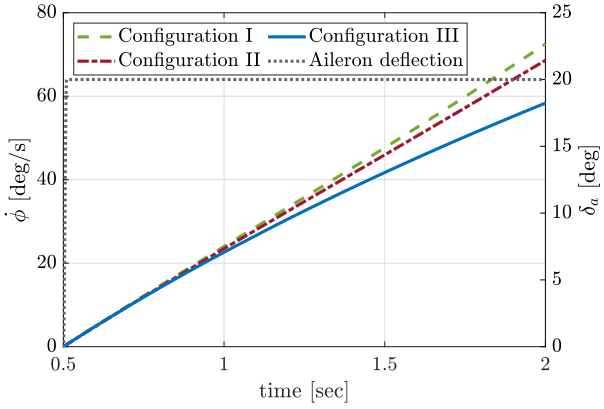

Figure 11: Comparison of the roll rate evolution.

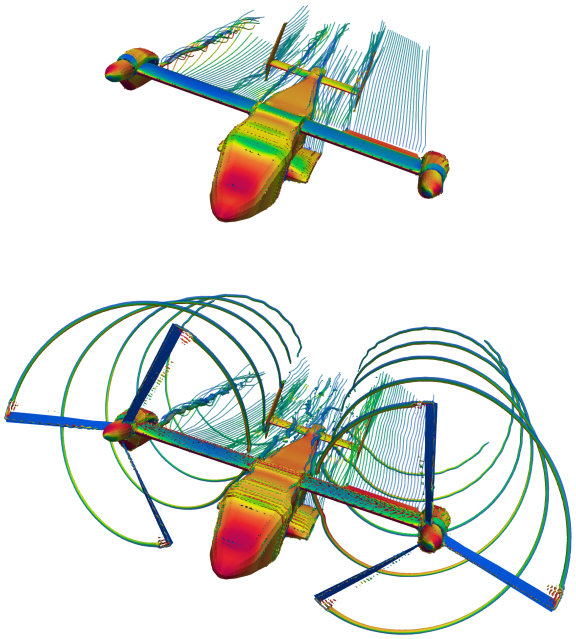

Figure 12: Representation of XV-15 tiltrotor wake for Configuration II and Configuration III [11]

In order to evaluate the roll manoeuvre performance for the different configurations tested, Tab. 7 reports the percentage differences between the time to bank an angle equal to 45° computed for aircraft Configurations I and II and the one computed for the complete aircraft equipped with rotors, i.e. Configuration III.

Configuration	Δ%
Configuration I	-4.46 %
Configuration II	-3.33 %

Table 7: Comparison of the differences Δ% between the time to bank 45° for aircraft Configurations I and II and Configuration III.

The coupled simulations results show that the introduction of rotors decreases the roll performance manoeuvre. Indeed, as shown from the comparison of roll rate evolution ($\dot{\phi}$) presented in Fig. 11, the rotor aerodynamic loads decrease the roll rate and produces a contrasting effect on the manoeuvre. This is related to the backward tilting of the rotor induced by the component of reference velocity associated with roll rate in the rotor's plane. Furthermore, the aircraft rolling motion causes an opposite variation of the thrust of the two rotors, as reported in Fig. 13.

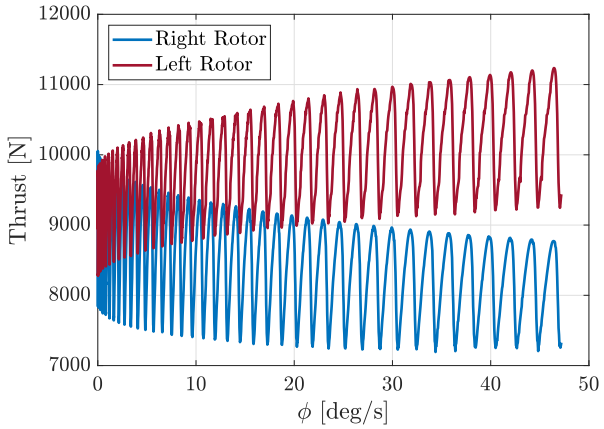

Figure 13: Comparison on thrust of the two rotors with respect to bank angle during the roll manoeuvre.

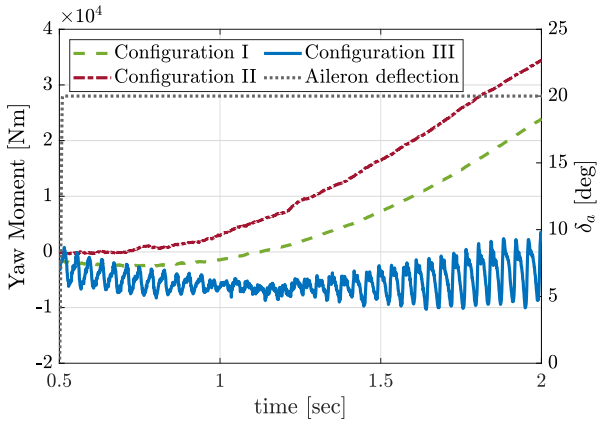

Figure 14: Comparison of the yawing moment evolution during the roll manoeuvre.

The Fig. 14 shows the yaw moment measured as a constraint reaction to the ground joint. Since the position of this constraint is fixed during the simulation, the purpose of these results is not to establish the actual behavior of the aircraft but to estimate the impact of the different parts on this magnitude. The analysis shows that tailplanes generate a proverse contribution compared to the simplest Configuration I. On the other hand, the introduction of the rotors aerodynamics contribution introduces an adverse yaw moment. This effect is related to the opposite variation of the two rotors thrust highlighted in Fig. 13.

Considering dynamic oscillations of aircraft during the roll manoeuvre, a quite complex response is observed for full aircraft configuration with rotors, i.e. Configuration III. In particular, the Fast Fourier Transform of the yawing moment time history computed for Configuration III shown in Fig. 15 clearly identify the correspondence of these oscillations with the multiples of the rotor n/rev.

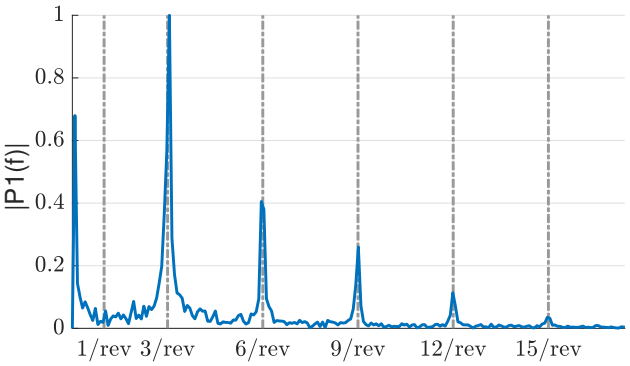

Figure 15: Fourier transform of yaw moment time history for Configuration III

4 CONCLUSIONS

The present work presented the capability of a novel aeroelastic numerical tool obtained by joining the multibody solver MBDyn with the mid-fidelity aerodynamic solver DUST to simulate the roll manoeuvre of a complete tiltrotor. The validation of the coupled tool over a simple wing and a single rotor in hover shows that the accurate description of aerodynamics made by means of VPM modelling of wakes enables to obtain a more accurate representation of rotorcraft performance. Then, the coupled simulations of the roll manoeuvre for different tiltrotor configurations enabled to appreciate the effects of both tailplanes and rotors wake to roll maneouvre performance and to aircraft yawing moment evolution. The coupled tool can be therefore considered in a mature state to be used for the investigation of the performance of novel rotorcraft configurations during manoeuvres. Future developments of the present work will include the possibility to perform coupled simulations increasing the complexity of the model, i.e. with the entire tiltrotor model equipped with flexible deformable wing, tailplanes and rotors. Moreover, further development will include the simulations of the tiltrotor maneuver in free flight by introducing a control for the management of the trim.

5 ACKNOWLEDGMENTS

The research leading to these results has received funding from the Clean Sky 2 – H2020 Framework Programme, under the grant agreement N.885971, (FORMOSA project).

Copyright Statement

holder of this paper, for the publication and distribution of this paper as part of the ERF proceedings or as individual offprints from the proceedings and for inclusion in a freely accessible web-based repository.

REFERENCES

[1] M. Maisel. NASA/Army XV-15 tilt-rotor research aircraft familiarization document. TM X-62,407, NASA, January 1975.

[2] GB Churchill and RM Gerdes. Advanced afcs developments on the xv-15 tilt rotor research aircraft.[automatic flight control system]. 1984.

[3] Georges-Henri Cottet, Petros D Koumoutsakos, D Petros, et al. *Vortex methods: theory and practice*. Cambridge University Press, 2000.

[4] Gian Luca Ghiringhelli, Pierangelo Masarati, Paolo Mantegazza, and Mark W. Nixon. Multi-body analysis of a tiltrotor configuration. *Nonlinear Dynamics*, 19(4):333–357, August 1999. doi:10.1023/A:1008386219934.

[5] M. Mattaboni, P. Masarati, G. Quaranta, and P. Mantegazza. Multibody simulation of integrated tiltrotor flight mechanics, aeroelasticity and control. *J. of Guidance, Control, and Dynamics*, 35(5):1391–1405, September/October 2012. doi:10.2514/1.57309.

[6] Davide Montagnani, Matteo Tugnoli, Federico Fonte, Alex Zanotti, Monica Syal, and Giovanni Droandi. Mid-fidelity analysis of unsteady interactional aerodynamics of complex vtol configurations. In *45th European Rotorcraft Forum (ERF 2019)*, pages 1–11, 2019.

[7] Pierangelo Masarati and Giuseppe Quaranta. Bioaeroservoelastic analysis of involuntary rotorcraft-pilot interaction. *J. of Computational and Nonlinear Dynamics*, 9(3):031009, July 2014. doi:10.1115/1.4025354.

[8] Hans-Joachim Bungartz, Florian Lindner, Bernhard Gatzhammer, Miriam Mehl, Klaudius Scheufele, Alexander Shukaev, and Benjamin Uekermann. preCICE – a fully parallel library for multi-physics surface coupling. *Computers and Fluids*, 141:250–258, 2016. Advances in Fluid-Structure Interaction.

[9] Matteo Tugnoli, Davide Montagnani, Monica Syal, Giovanni Droandi, and Alex Zanotti. Mid-fidelity approach to aerodynamic simulations of unconventional vtol aircraft configurations. *Aerospace Science and Technology*, 115:106804, 2021.

[10] Alex Zanotti, Alberto Savino, Michele Palazzi, Matteo Tugnoli, and Vincenzo Muscarello. Assessment of a mid-fidelity numerical approach for the investigation of tiltrotor aerodynamics. *Applied Sciences*, 11(8):3385, 2021.

[11] A Cocco, A Savino, A Zanotti, A Zanoni, P Masarati, and V Muscarello. Coupled multibody-mid fidelity aerodynamic solver for tiltrotor aeroelastic simulation. In *9th International Conference on Computational Methods for Coupled Problems in Science and Engineering, COUPLED PROBLEMS 2021*, pages 1–12. CIMNE, 2021.

[12] Martin Goland. The flutter of a uniform cantilever wing. *Journal of Applied Mechanics-Transactions of the Asme*, 12(4):A197–A208, 1945.

[13] Gian Luca Ghiringhelli, Pierangelo Masarati, and Paolo Mantegazza. Characterisation of a smart rotor blade incorporating active fibre composites. In *Smart Structures and Materials 2000*, pages 119–128, Madrid, Spain, June 19–21 2000.

[14] Zhicun Wang, PC Chen, DD Liu, DT Mook, and MJ Patil. Time domain nonlinear aeroelastic analysis for hale wings. In *47th AIAA/ASME/ASCE/AHS/ASC Structures, Structural Dynamics, and Materials Conference 14th AIAA/ASME/AHS Adaptive Structures Conference 7th*, page 1640, 2006.

[15] Joseba Murua, Rafael Palacios, and J Michael R Graham. Assessment of wake-tail interference effects on the dynamics of flexible aircraft. *AIAA Journal*, 50(7):1575–1585, 2012.

[16] CW Acree Jr. An improved camrad model for aeroelastic stability analysis of the xv-15 with advanced technology blades. 1993.

[17] Gian Luca Ghiringhelli, Pierangelo Masarati, and Paolo Mantegazza. A multi-body implementation of finite volume beams. *AIAA Journal*, 38(1):131–138, January 2000. doi:10.2514/2.933.

[18] C. W. Acree, R. J. Peyran, and Wayne Johnson. Rotor design options for improving tiltrotor whirl-flutter stability margins. *Journal of the American Helicopter Society*, 46(2):87–95, April 2001. doi:10.4050/JAHS.56.022004.

[19] David B. Signor Fort F. Felker, Mark D. Betzina. Performance and loads data from a hover test of a full-scale xv-15 rotor. Technical report, NASA Ames Research Center, Moffett Field California, 1985.

[20] Joon Lim and Steven Tran. Interactional structural loads of the xv-15 rotor in airplane mode. In *45th European Rotorcraft Forum (ERF 2019)*, pages 1–10, 2019.

[21] Samuel W. Ferguson. Development and validation of a simulation for a generic tilt-rotor aircraft. CR 166537, NASA, 1989.